

Laser Beams and Resonators

H. KOGELNIK AND T. LI

Abstract—This paper is a review of the theory of laser beams and resonators. It is meant to be tutorial in nature and useful in scope. No attempt is made to be exhaustive in the treatment. Rather, emphasis is placed on formulations and derivations which lead to basic understanding and on results which bear practical significance.

1. INTRODUCTION

THE COHERENT radiation generated by lasers or masers operating in the optical or infrared wavelength regions usually appears as a beam whose transverse extent is large compared to the wavelength. The resonant properties of such a beam in the resonator structure, its propagation characteristics in free space, and its interaction behavior with various optical elements and devices have been studied extensively in recent years. This paper is a review of the theory of laser beams and resonators. Emphasis is placed on formulations and derivations which lead to basic understanding and on results which are of practical value.

Historically, the subject of laser resonators had its origin when Dicke [1], Prokhorov [2], and Schawlow and Townes [3] independently proposed to use the Fabry-Perot interferometer as a laser resonator. The modes in such a structure, as determined by diffraction effects, were first calculated by Fox and Li [4]. Boyd and Gordon [5], and Boyd and Kogelnik [6] developed a theory for resonators with spherical mirrors and approximated the modes by wave beams. The concept of electromagnetic wave beams was also introduced by Goubau and Schwering [7], who investigated the properties of sequences of lenses for the guided transmission of electromagnetic waves. Another treatment of wave beams was given by Pierce [8]. The behavior of Gaussian laser beams as they interact with various optical structures has been analyzed by Goubau [9], Kogelnik [10], [11], and others.

The present paper summarizes the various theories and is divided into three parts. The first part treats the passage of paraxial rays through optical structures and is based on geometrical optics. The second part is an analysis of laser beams and resonators, taking into account the wave nature of the beams but ignoring diffraction effects due to the finite size of the apertures. The third part treats the resonator modes, taking into account aperture diffraction effects. Whenever applicable, useful results are presented in the forms of formulas, tables, charts, and graphs.

Manuscript received July 12, 1966.

H. Kogelnik is with Bell Telephone Laboratories, Inc., Murray Hill, N. J.

T. Li is with Bell Telephone Laboratories, Inc., Holmdel, N. J.

2. PARAXIAL RAY ANALYSIS

A study of the passage of paraxial rays through optical resonators, transmission lines, and similar structures can reveal many important properties of these systems. One such "geometrical" property is the stability of the structure [6], another is the loss of unstable resonators [12]. The propagation of paraxial rays through various optical structures can be described by ray transfer matrices. Knowledge of these matrices is particularly useful as they also describe the propagation of Gaussian beams through these structures; this will be discussed in Section 3. The present section describes briefly some ray concepts which are useful in understanding laser beams and resonators, and lists the ray matrices of several optical systems of interest. A more detailed treatment of ray propagation can be found in textbooks [13] and in the literature on laser resonators [14].

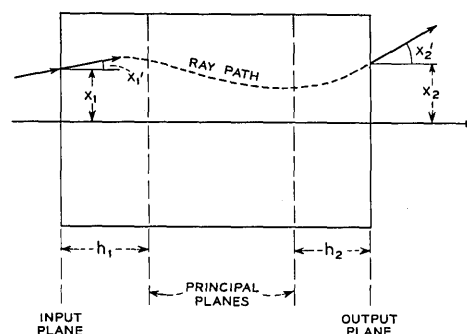


Fig. 1. Reference planes of an optical system. A typical ray path is indicated.

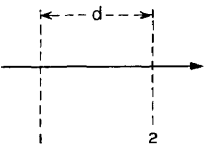
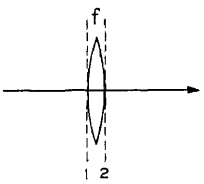
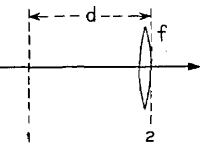
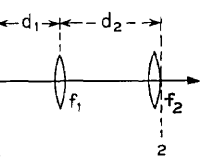
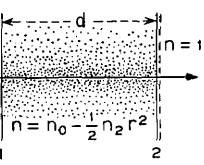
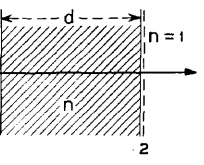
2.1 Ray Transfer Matrix

A paraxial ray in a given cross section ($z = \text{const}$) of an optical system is characterized by its distance x from the optic (z) axis and by its angle or slope x' with respect to that axis. A typical ray path through an optical structure is shown in Fig. 1. The slope x' of paraxial rays is assumed to be small. The ray path through a given structure depends on the optical properties of the structure and on the input conditions, i.e., the position x_1 and the slope x_1' of the ray in the input plane of the system. For paraxial rays the corresponding output quantities x_2 and x_2' are linearly dependent on the input quantities. This is conveniently written in the matrix form

$$\begin{bmatrix} x_2 \\ x_2' \end{bmatrix} = \begin{bmatrix} A & B \\ C & D \end{bmatrix} \begin{bmatrix} x_1 \\ x_1' \end{bmatrix} \quad (1)$$

TABLE I

RAY TRANSFER MATRICES OF SIX ELEMENTARY OPTICAL STRUCTURES

NO	OPTICAL SYSTEM	RAY TRANSFER MATRIX
1		$\begin{vmatrix} 1 & d \\ 0 & 1 \end{vmatrix}$
2		$\begin{vmatrix} 1 & 0 \\ -\frac{1}{f} & 1 \end{vmatrix}$
3		$\begin{vmatrix} 1 & d \\ -\frac{1}{f} & 1 - \frac{d}{f} \end{vmatrix}$
4		$\begin{vmatrix} 1 - \frac{d_2}{f_1} & d_1 + d_2 - \frac{d_1 d_2}{f_1} \\ -\frac{1}{f_1} - \frac{1}{f_2} + \frac{d_2}{f_1 f_2} & 1 - \frac{d_1}{f_1} - \frac{d_2}{f_2} - \frac{d_1}{f_2} + \frac{d_1 d_2}{f_1 f_2} \end{vmatrix}$
5		$\begin{vmatrix} \cos d \sqrt{\frac{n_2}{n_0}} & \frac{1}{\sqrt{n_0 n_2}} \sin d \sqrt{\frac{n_2}{n_0}} \\ -\sqrt{n_0 n_2} \sin d \sqrt{\frac{n_2}{n_0}} & \cos d \sqrt{\frac{n_2}{n_0}} \end{vmatrix}$
6		$\begin{vmatrix} 1 & d/n \\ 0 & 1 \end{vmatrix}$

where the slopes are measured positive as indicated in the figure. The $ABCD$ matrix is called the ray transfer matrix. Its determinant is generally unity

$$AD - BC = 1. \quad (2)$$

The matrix elements are related to the focal length f of the system and to the location of the principal planes by

$$f = -\frac{1}{C}$$

$$h_1 = \frac{D - 1}{C} \quad (3)$$

$$h_2 = \frac{A - 1}{C}$$

where h_1 and h_2 are the distances of the principal planes from the input and output planes as shown in Fig. 1.

In Table I there are listed the ray transfer matrices of six elementary optical structures. The matrix of No. 1 describes the ray transfer over a distance d . No. 2 describes the transfer of rays through a thin lens of focal length f . Here the input and output planes are immediately to the left and right of the lens. No. 3 is a combination of the first two. It governs rays passing first over a distance d and then through a thin lens. If the sequence is reversed the diagonal elements are interchanged. The matrix of No. 4 describes the rays passing through two structures of the No. 3 type. It is obtained by matrix multiplication. The ray transfer matrix for a lenslike medium of length d is given in No. 5. In this medium the refractive index varies quadratically with the distance r from the optic axis.

$$n = n_0 - \frac{1}{2} n_2 r^2. \quad (4)$$

An index variation of this kind can occur in laser crystals and in gas lenses. The matrix of a dielectric material of index n and length d is given in No. 6. The matrix is referred to the surrounding medium of index 1 and is computed by means of Snell's law. Comparison with No. 1 shows that for paraxial rays the effective distance is *shortened* by the optically denser material, while, as is well known, the "optical distance" is lengthened.

2.2 Periodic Sequences

Light rays that bounce back and forth between the spherical mirrors of a laser resonator experience a periodic focusing action. The effect on the rays is the same as in a periodic sequence of lenses [15] which can be used as an optical transmission line. A periodic sequence of identical optical systems is schematically indicated in Fig. 2. A single element of the sequence is characterized by its $ABCD$ matrix. The ray transfer through n consecutive elements of the sequence is described by the n th power of this matrix. This can be evaluated by means of Sylvester's theorem

$$\begin{vmatrix} A & B \\ C & D \end{vmatrix}^n = \frac{1}{\sin \Theta} \quad (5)$$

$$\begin{vmatrix} A \sin n\Theta - \sin(n-1)\Theta & B \sin n\Theta \\ C \sin n\Theta & D \sin n\Theta - \sin(n-1)\Theta \end{vmatrix}$$

where

$$\cos \Theta = \frac{1}{2}(A + D). \quad (6)$$

Periodic sequences can be classified as either *stable* or *unstable*. Sequences are stable when the trace $(A + D)$ obeys the inequality

$$-1 < \frac{1}{2}(A + D) < 1. \quad (7)$$

Inspection of (5) shows that rays passing through a stable sequence are periodically refocused. For unstable systems, the trigonometric functions in that equation become hyperbolic functions, which indicates that the rays become more and more dispersed the further they pass through the sequence.

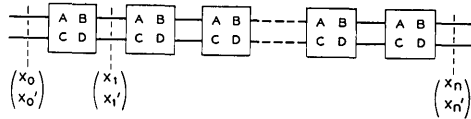


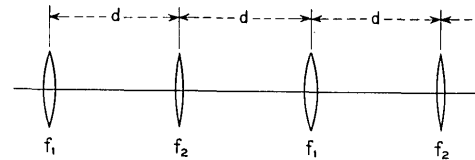
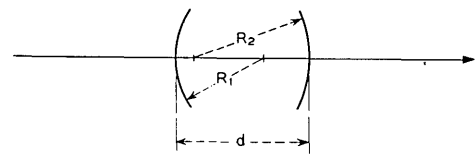
Fig. 2. Periodic sequence of identical systems, each characterized by its $ABCD$ matrix.

2.3 Stability of Laser Resonators

A laser resonator with spherical mirrors of unequal curvature is a typical example of a periodic sequence that can be either stable or unstable [6]. In Fig. 3 such a resonator is shown together with its dual, which is a sequence of lenses. The ray paths through the two structures are the same, except that the ray pattern is folded in the resonator and unfolded in the lens sequence. The focal lengths f_1 and f_2 of the lenses are the same as the focal lengths of the mirrors, i.e., they are determined by the radii of curvature R_1 and R_2 of the mirrors ($f_1 = R_1/2$, $f_2 = R_2/2$). The lens spacings are the same as the mirror spacing d . One can choose, as an element of the periodic sequence, a spacing followed by one lens plus another spacing followed by the second lens. The $ABCD$ matrix of such an element is given in No. 4 of Table I. From this one can obtain the trace, and write the stability condition (7) in the form

$$0 < \left(1 - \frac{d}{R_1}\right) \left(1 - \frac{d}{R_2}\right) < 1. \quad (8)$$

To show graphically which type of resonator is stable and which is unstable, it is useful to plot a stability diagram on which each resonator type is represented by a point. This is shown in Fig. 4 where the parameters d/R_1 and d/R_2 are drawn as the coordinate axes; unstable systems are represented by points in the shaded areas. Various resonator types, as characterized by the relative positions of the centers of curvature of the mirrors, are indicated in the appropriate regions of the diagram. Also entered as alternate coordinate axes are the parameters g_1 and g_2 which play an important role in the diffraction theory of resonators (see Section 4).



$$R_1 = 2f_1, \quad R_2 = 2f_2$$

Fig. 3. Spherical-mirror resonator and the equivalent sequence of lenses.

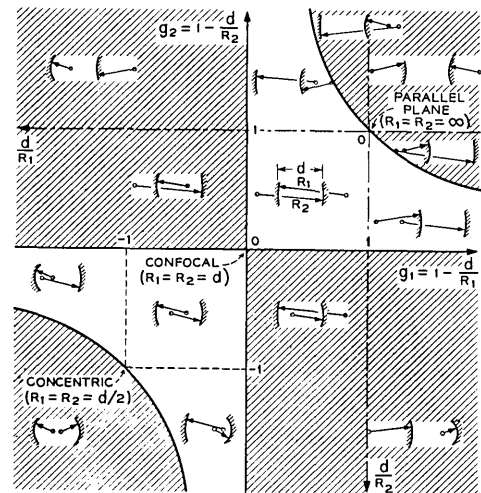


Fig. 4. Stability diagram. Unstable resonator systems lie in shaded regions.

3. WAVE ANALYSIS OF BEAMS AND RESONATORS

In this section the wave nature of laser beams is taken into account, but diffraction effects due to the finite size of apertures are neglected. The latter will be discussed in Section 4. The results derived here are applicable to optical systems with "large apertures," i.e., with apertures that intercept only a negligible portion of the beam power. A theory of light beams or "beam waves" of this kind was first given by Boyd and Gordon [5] and by Goubau and Schwering [7]. The present discussion follows an analysis given in [11].

3.1 Approximate Solution of the Wave Equation

Laser beams are similar in many respects to plane waves; however, their intensity distributions are not uniform, but are concentrated near the axis of propagation and their phase fronts are slightly curved. A field component or potential u of the coherent light satisfies the scalar wave equation

$$\nabla^2 u + k^2 u = 0 \quad (9)$$

where $k = 2\pi/\lambda$ is the propagation constant in the medium.

For light traveling in the z direction one writes

$$u = \psi(x, y, z) \exp(-jkz) \quad (10)$$

where ψ is a slowly varying complex function which represents the differences between a laser beam and a plane wave, namely: a nonuniform intensity distribution, expansion of the beam with distance of propagation, curvature of the phase front, and other differences discussed below. By inserting (10) into (9) one obtains

$$\frac{\partial^2 \psi}{\partial x^2} + \frac{\partial^2 \psi}{\partial y^2} - 2jk \frac{\partial \psi}{\partial z} = 0 \quad (11)$$

where it has been assumed that ψ varies so slowly with z that its second derivative $\partial^2 \psi / \partial z^2$ can be neglected.

The differential equation (11) for ψ has a form similar to the time dependent Schrödinger equation. It is easy to see that

$$\psi = \exp \left\{ -j \left(P + \frac{k}{2q} r^2 \right) \right\} \quad (12)$$

is a solution of (11), where

$$r^2 = x^2 + y^2. \quad (13)$$

The parameter $P(z)$ represents a *complex* phase shift which is associated with the propagation of the light beam, and $q(z)$ is a *complex* beam parameter which describes the Gaussian variation in beam intensity with the distance r from the optic axis, as well as the curvature of the phase front which is spherical near the axis. After insertion of (12) into (11) and comparing terms of equal powers in r one obtains the relations

$$q' = 1 \quad (14)$$

and

$$P' = -\frac{j}{q} \quad (15)$$

where the prime indicates differentiation with respect to z . The integration of (14) yields

$$q_2 = q_1 + z \quad (16)$$

which relates the beam parameter q_2 in one plane (output plane) to the parameter q_1 in a second plane (input plane) separated from the first by a distance z .

3.2 Propagation Laws for the Fundamental Mode

A coherent light beam with a Gaussian intensity profile as obtained above is not the only solution of (11), but is perhaps the most important one. This beam is often called the "fundamental mode" as compared to the higher order modes to be discussed later. Because of its importance it is discussed here in greater detail.

For convenience one introduces two *real* beam parameters R and w related to the complex parameter q by

$$\frac{1}{q} = \frac{1}{R} - j \frac{\lambda}{\pi w^2}. \quad (17)$$

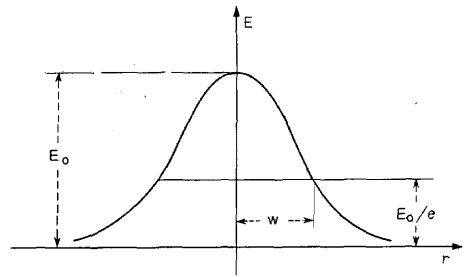


Fig. 5. Amplitude distribution of the fundamental beam.

When (17) is inserted in (12) the physical meaning of these two parameters becomes clear. One sees that $R(z)$ is the radius of curvature of the wavefront that intersects the axis at z , and $w(z)$ is a measure of the decrease of the field amplitude E with the distance from the axis. This decrease is Gaussian in form, as indicated in Fig. 5, and w is the distance at which the amplitude is $1/e$ times that on the axis. Note that the intensity distribution is Gaussian in every beam cross section, and that the width of that Gaussian intensity profile changes along the axis. The parameter w is often called the beam radius or "spot size," and $2w$, the beam diameter.

The Gaussian beam contracts to a minimum diameter $2w_0$ at the *beam waist* where the phase front is plane. If one measures z from this waist, the expansion laws for the beam assume a simple form. The complex beam parameter at the waist is purely imaginary

$$q_0 = j \frac{\pi w_0^2}{\lambda} \quad (18)$$

and a distance z away from the waist the parameter is

$$q = q_0 + z = j \frac{\pi w_0^2}{\lambda} + z. \quad (19)$$

After combining (19) and (17) one equates the real and imaginary parts to obtain

$$w^2(z) = w_0^2 \left[1 + \left(\frac{\lambda z}{\pi w_0^2} \right)^2 \right] \quad (20)$$

and

$$R(z) = z \left[1 + \left(\frac{\pi w_0^2}{\lambda z} \right)^2 \right]. \quad (21)$$

Figure 6 shows the expansion of the beam according to (20). The beam contour $w(z)$ is a hyperbola with asymptotes inclined to the axis at an angle

$$\theta = \frac{\lambda}{\pi w_0}. \quad (22)$$

This is the far-field diffraction angle of the fundamental mode.

Dividing (21) by (20), one obtains the useful relation

$$\frac{\lambda z}{\pi w_0^2} = \frac{\pi w^2}{\lambda R} \quad (23)$$

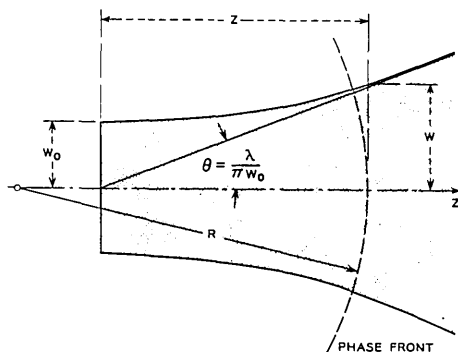


Fig. 6. Contour of a Gaussian beam.

which can be used to express w_0 and z in terms of w and R :

$$w_0^2 = w^2 / \left[1 + \left(\frac{\pi w^2}{\lambda R} \right)^2 \right] \quad (24)$$

$$z = R / \left[1 + \left(\frac{\lambda R}{\pi w^2} \right)^2 \right]. \quad (25)$$

To calculate the complex phase shift a distance z away from the waist, one inserts (19) into (15) to get

$$P' = -\frac{j}{q} = -\frac{j}{z + j(\pi w_0^2/\lambda)} \quad (26)$$

Integration of (26) yields the result

$$\begin{aligned} jP(z) &= \ln[1 - j(\lambda z/\pi w_0^2)] \\ &= \ln\sqrt{1 + (\lambda z/\pi w_0^2)^2} - j \arctan(\lambda z/\pi w_0^2). \end{aligned} \quad (27)$$

The real part of P represents a phase shift difference Φ between the Gaussian beam and an ideal plane wave, while the imaginary part produces an amplitude factor w_0/w which gives the expected intensity decrease on the axis due to the expansion of the beam. With these results for the fundamental Gaussian beam, (10) can be written in the form

$$\begin{aligned} u(r, z) &= \frac{w_0}{w} \\ &\cdot \exp \left\{ -j(kz - \Phi) - r^2 \left(\frac{1}{w^2} + \frac{jk}{2R} \right) \right\} \end{aligned} \quad (28)$$

where

$$\Phi = \arctan(\lambda z/\pi w_0^2). \quad (29)$$

It will be seen in Section 3.5 that Gaussian beams of this kind are produced by many lasers that oscillate in the fundamental mode.

3.3 Higher Order Modes

In the preceding section only one solution of (11) was discussed, i.e., a light beam with the property that its intensity profile in every beam cross section is given by the same function, namely, a Gaussian. The width of this Gaussian distribution changes as the beam propagates along its axis. There are other solutions of (11) with sim-

ilar properties, and they are discussed in this section. These solutions form a complete and orthogonal set of functions and are called the "modes of propagation." Every arbitrary distribution of monochromatic light can be expanded in terms of these modes. Because of space limitations the derivation of these modes can only be sketched here.

a) *Modes in Cartesian Coordinates:* For a system with a rectangular (x, y, z) geometry one can try a solution for (11) of the form

$$\begin{aligned} \psi &= g\left(\frac{x}{w}\right) \cdot h\left(\frac{y}{w}\right) \\ &\cdot \exp \left\{ -j \left[P + \frac{k}{2q} (x^2 + y^2) \right] \right\} \end{aligned} \quad (30)$$

where g is a function of x and z , and h is a function of y and z . For real g and h this postulates mode beams whose intensity patterns scale according to the width $2w(z)$ of a Gaussian beam. After inserting this trial solution into (11) one arrives at differential equations for g and h of the form

$$\frac{d^2 H_m}{dx^2} - 2x \frac{dH_m}{dx} + 2mH_m = 0. \quad (31)$$

This is the differential equation for the Hermite polynomial $H_m(x)$ of order m . Equation (11) is satisfied if

$$g \cdot h = H_m \left(\sqrt{2} \frac{x}{w} \right) H_n \left(\sqrt{2} \frac{y}{w} \right) \quad (32)$$

where m and n are the (transverse) mode numbers. Note that the same pattern scaling parameter $w(z)$ applies to modes of all orders.

Some Hermite polynomials of low order are

$$\begin{aligned} H_0(x) &= 1 \\ H_1(x) &= x \\ H_2(x) &= 4x^2 - 2 \\ H_3(x) &= 8x^3 - 12x. \end{aligned} \quad (33)$$

Expression (28) can be used as a mathematical description of higher order light beams, if one inserts the product $g \cdot h$ as a factor on the right-hand side. The intensity pattern in a cross section of a higher order beam is, thus, described by the product of Hermite and Gaussian functions. Photographs of such mode patterns are shown in Fig. 7. They were produced as modes of oscillation in a gas laser oscillator [16]. Note that the number of zeros in a mode pattern is equal to the corresponding mode number, and that the area occupied by a mode increases with the mode number.

The parameter $R(z)$ in (28) is the same for all modes, implying that the phase-front curvature is the same and changes in the same way for modes of all orders. The phase shift Φ , however, is a function of the mode numbers. One obtains

$$\Phi(m, n; z) = (m + n + 1) \arctan(\lambda z/\pi w_0^2). \quad (34)$$

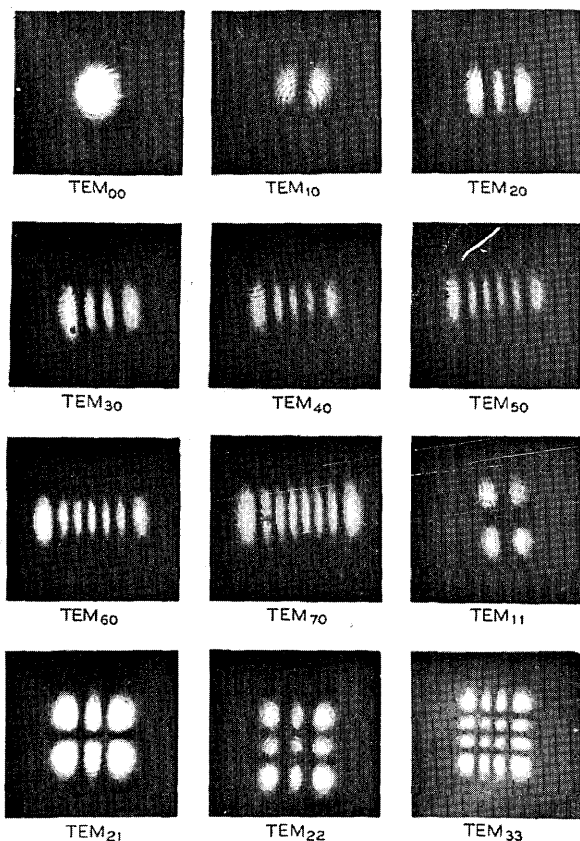


Fig. 7. Mode patterns of a gas laser oscillator (rectangular symmetry).

This means that the phase velocity increases with increasing mode number. In resonators this leads to differences in the resonant frequencies of the various modes of oscillation.

b) *Modes in Cylindrical Coordinates:* For a system with a cylindrical (r, ϕ, z) geometry one uses a trial solution for (11) of the form

$$\psi = g\left(\frac{r}{w}\right) \cdot \exp\left\{-j\left(P + \frac{k}{2q}r^2 + l\phi\right)\right\}. \quad (35)$$

After some calculation one finds

$$g = \left(\sqrt{2} \frac{r}{w}\right)^l \cdot L_p^l\left(2 \frac{r^2}{w^2}\right) \quad (36)$$

where L_p^l is a generalized Laguerre polynomial, and p and l are the radial and angular mode numbers. $L_p^l(x)$ obeys the differential equation

$$x \frac{d^2 L_p^l}{dx^2} + (l+1-x) \frac{dL_p^l}{dx} + pL_p^l = 0. \quad (37)$$

Some polynomials of low order are

$$\begin{aligned} L_0^l(x) &= 1 \\ L_1^l(x) &= l+1-x \\ L_2^l(x) &= \frac{1}{2}(l+1)(l+2) - (l+2)x + \frac{1}{2}x^2. \end{aligned} \quad (38)$$

As in the case of beams with a rectangular geometry, the beam parameters $w(z)$ and $R(z)$ are the same for all cylindrical modes. The phase shift is, again, dependent on the mode numbers and is given by

$$\Phi(p, l; z) = (2p + l + 1) \arctan(\lambda z / \pi w_0^2). \quad (39)$$

3.4 Beam Transformation by a Lens

A lens can be used to focus a laser beam to a small spot, or to produce a beam of suitable diameter and phase-front curvature for injection into a given optical structure. An ideal lens leaves the transverse field distribution of a beam mode unchanged, i.e., an incoming fundamental Gaussian beam will emerge from the lens as a fundamental beam, and a higher order mode remains a mode of the same order after passing through the lens. However, a lens does change the beam parameters $R(z)$ and $w(z)$. As these two parameters are the same for modes of all orders, the following discussion is valid for all orders; the relationship between the parameters of an incoming beam (labeled here with the index 1) and the parameters of the corresponding outgoing beam (index 2) is studied in detail.

An ideal thin lens of focal length f transforms an incoming spherical wave with a radius R_1 immediately to the left of the lens into a spherical wave with the radius R_2 immediately to the right of it, where

$$\frac{1}{R_2} = \frac{1}{R_1} - \frac{1}{f}. \quad (40)$$

Figure 8 illustrates this situation. The radius of curvature is taken to be positive if the wavefront is convex as viewed from $z = \infty$. The lens transforms the phase fronts of laser beams in exactly the same way as those of spherical waves. As the diameter of a beam is the same immediately to the left and to the right of a *thin* lens, the q -parameters of the incoming and outgoing beams are related by

$$\frac{1}{q_2} = \frac{1}{q_1} - \frac{1}{f}, \quad (41)$$

where the q 's are measured at the lens. If q_1 and q_2 are measured at distances d_1 and d_2 from the lens as indicated in Fig. 9, the relation between them becomes

$$q_2 = \frac{(1 - d_2/f)q_1 + (d_1 + d_2 - d_1 d_2/f)}{-(q_1/f) + (1 - d_1/f)}. \quad (42)$$

This formula is derived using (16) and (41).

More complicated optical structures, such as gas lenses, combinations of lenses, or thick lenses, can be thought of as composed of a series of thin lenses at various spacings. Repeated application of (16) and (41) is, therefore, sufficient to calculate the effect of complicated structures on the propagation of laser beams. If the $ABCD$ matrix for the transfer of paraxial rays through the structure is known, the q parameter of the output beam can be calculated from

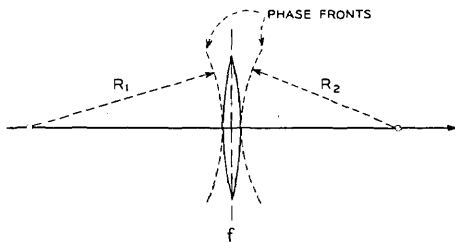


Fig. 8. Transformation of wavefronts by a thin lens.

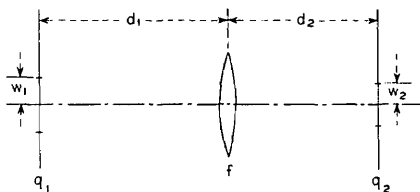


Fig. 9. Distances and parameters for a beam transformed by a thin lens.

$$q_2 = \frac{Aq_1 + B}{Cq_1 + D} \quad (43)$$

This is a generalized form of (42) and has been called the *ABCD* law [10]. The matrices of several optical structures are given in Section II. The *ABCD* law follows from the analogy between the laws for laser beams and the laws obeyed by the spherical waves in geometrical optics. The radius of the spherical waves R obeys laws of the same form as (16) and (41) for the complex beam parameter q . A more detailed discussion of this analogy is given in [11].

3.5 Laser Resonators (Infinite Aperture)

The most commonly used laser resonators are composed of two spherical (or flat) mirrors facing each other. The stability of such "open" resonators has been discussed in Section 2 in terms of paraxial rays. To study the *modes* of laser resonators one has to take account of their wave nature, and this is done here by studying wave beams of the kind discussed above as they propagate back and forth between the mirrors. As aperture diffraction effects are neglected throughout this section, the present discussion applies only to stable resonators with mirror apertures that are large compared to the spot size of the beams.

A mode of a resonator is defined as a self-consistent field configuration. If a mode can be represented by a wave beam propagating back and forth between the mirrors, the beam parameters must be the same after one complete return trip of the beam. This condition is used to calculate the mode parameters. As the beam that represents a mode travels in both directions between the mirrors it forms the axial standing-wave pattern that is expected for a resonator mode.

A laser resonator with mirrors of equal curvature is shown in Fig. 10 together with the equivalent unfolded system, a sequence of lenses. For this symmetrical structure it is sufficient to postulate self-consistency for one transit of the resonator (which is equivalent to one full period of the lens sequence), instead of a complete return

trip. If the complex beam parameter is given by q_1 , immediately to the right of a particular lens, the beam parameter q_2 , immediately to the right of the next lens, can be calculated by means of (16) and (41) as

$$\frac{1}{q_2} = \frac{1}{q_1 + d} - \frac{1}{f} \quad (44)$$

Self-consistency requires that $q_1 = q_2 = q$, which leads to a quadratic equation for the beam parameter q at the lenses (or at the mirrors of the resonator):

$$\frac{1}{q^2} + \frac{1}{fq} + \frac{1}{fd} = 0 \quad (45)$$

The roots of this equation are

$$\frac{1}{q} = -\frac{1}{2f} (+) j \sqrt{\frac{1}{fd} - \frac{1}{4f^2}} \quad (46)$$

where only the root that yields a real beamwidth is used. (Note that one gets a real beamwidth for stable resonators only.)

From (46) one obtains immediately the real beam parameters defined in (17). One sees that R is equal to the radius of curvature of the mirrors, which means that the mirror surfaces are coincident with the phase fronts of the resonator modes. The width $2w$ of the fundamental mode is given by

$$w^2 = \left(\frac{\lambda R}{\pi} \right) / \sqrt{2 \frac{R}{d} - 1} \quad (47)$$

To calculate the beam radius w_0 in the center of the resonator where the phase front is plane, one uses (23) with $z = d/2$ and gets

$$w_0^2 = \frac{\lambda}{2\pi} \sqrt{d(2R - d)} \quad (48)$$

The beam parameters R and w describe the modes of all orders. But the phase velocities are different for the different orders, so that the resonant conditions depend on the mode numbers. Resonance occurs when the phase shift from one mirror to the other is a multiple of π . Using (28) and (34) this condition can be written as

$$kd - 2(m + n + 1) \arctan(\lambda d / 2\pi w_0^2) = \pi(q + 1) \quad (49)$$

where q is the number of nodes of the axial standing-wave pattern (the number of half wavelengths is $q + 1$),¹ and m and n are the rectangular mode numbers defined in Section 3.3. For the modes of circular geometry one obtains a similar condition where $(2p + l + 1)$ replaces $(m + n + 1)$.

The fundamental beat frequency ν_0 , i.e., the frequency spacing between successive longitudinal resonances, is given by

$$\nu_0 = c/2d \quad (50)$$

¹ This q is not to be confused with the complex beam parameter.

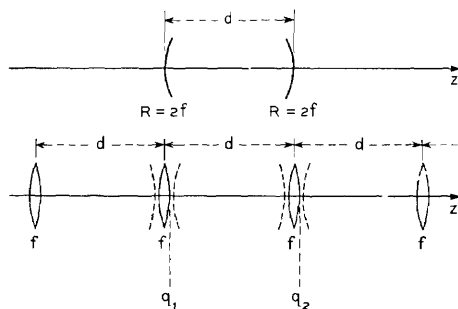


Fig. 10. Symmetrical laser resonator and the equivalent sequence of lenses. The beam parameters, q_1 and q_2 , are indicated.

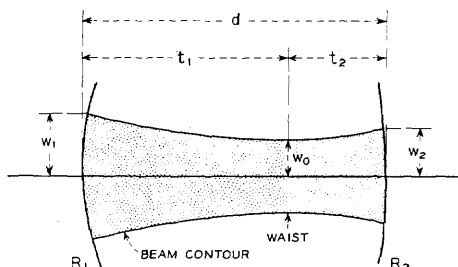


Fig. 11. Mode parameters of interest for a resonator with mirrors of unequal curvature.

where c is the velocity of light. After some algebraic manipulations one obtains from (49) the following formula for the resonant frequency ν of a mode

$$\nu/\nu_0 = (q+1) + \frac{1}{\pi} (m+n+1) \arccos(1-d/R). \quad (51)$$

For the special case of the confocal resonator ($d=R=b$), the above relations become

$$w^2 = \lambda b/\pi, \quad w_0^2 = \lambda b/2\pi; \\ \nu/\nu_0 = (q+1) + \frac{1}{2}(m+n+1). \quad (52)$$

The parameter b is known as the confocal parameter.

Resonators with mirrors of unequal curvature can be treated in a similar manner. The geometry of such a resonator where the radii of curvature of the mirrors are R_1 and R_2 is shown in Fig. 11. The diameters of the beam at the mirrors of a stable resonator, $2w_1$ and $2w_2$, are given by

$$w_1^4 = (\lambda R_1/\pi)^2 \frac{R_2 - d}{R_1 - d} \frac{d}{R_1 + R_2 - d} \\ w_2^4 = (\lambda R_2/\pi)^2 \frac{R_1 - d}{R_2 - d} \frac{d}{R_1 + R_2 - d}. \quad (53)$$

The diameter of the beam waist $2w_0$, which is formed either inside or outside the resonator, is given by

$$w_0^4 = \left(\frac{\lambda}{\pi}\right)^2 \frac{d(R_1 - d)(R_2 - d)(R_1 + R_2 - d)}{(R_1 + R_2 - 2d)^2}. \quad (54)$$

The distances t_1 and t_2 between the waist and the mirrors, measured positive as shown in the figure, are

$$t_1 = \frac{d(R_2 - d)}{R_1 + R_2 - 2d} \\ t_2 = \frac{d(R_1 - d)}{R_1 + R_2 - 2d}. \quad (55)$$

The resonant condition is

$$\nu/\nu_0 = (q+1) + \frac{1}{\pi} (m+n+1) \\ \arccos \sqrt{(1-d/R_1)(1-d/R_2)} \quad (56)$$

where the square root should be given the sign of $(1-d/R_1)$, which is equal to the sign of $(1-d/R_2)$ for a stable resonator.

There are more complicated resonator structures than the ones discussed above. In particular, one can insert a lens or several lenses between the mirrors. But in every case, the unfolded resonator is equivalent to a periodic sequence of identical optical systems as shown in Fig. 2. The elements of the $ABCD$ matrix of this system can be used to calculate the mode parameters of the resonator. One uses the $ABCD$ law (43) and postulates self-consistency by putting $q_1 = q_2 = q$. The roots of the resulting quadratic equation are

$$\frac{1}{q} = \frac{D-A}{2B} \pm \frac{j}{2B} \sqrt{4-(A+D)^2}, \quad (57)$$

which yields, for the corresponding beam radius w ,

$$w^2 = (2\lambda B/\pi)/\sqrt{4-(A+D)^2}. \quad (58)$$

3.6 Mode Matching

It was shown in the preceding section that the modes of laser resonators can be characterized by light beams with certain properties and parameters which are defined by the resonator geometry. These beams are often injected into other optical structures with different sets of beam parameters. These optical structures can assume various physical forms, such as resonators used in scanning Fabry-Perot interferometers or regenerative amplifiers, sequences of dielectric or gas lenses used as optical transmission lines, or crystals of nonlinear dielectric material employed in parametric optics experiments. To match the modes of one structure to those of another one must transform a given Gaussian beam (or higher order mode) into another beam with prescribed properties. This transformation is usually accomplished with a thin lens, but other more complex optical systems can be used. Although the present discussion is devoted to the simple case of the thin lens, it is also applicable to more complex systems, provided one measures the distances from the principal planes and uses the combined focal length f of the more complex system.

The location of the waists of the two beams to be transformed into each other and the beam diameters at the waists are usually known or can be computed. To match the beams one has to choose a lens of a focal length

f that is larger than a characteristic length f_0 defined by the two beams, and one has to adjust the distances between the lens and the two beam waists according to rules derived below.

In Fig. 9 the two beam waists are assumed to be located at distances d_1 and d_2 from the lens. The complex beam parameters at the waists are purely imaginary; they are

$$q_1 = j\pi w_1^2/\lambda, \quad q_2 = j\pi w_2^2/\lambda \quad (59)$$

where $2w_1$ and $2w_2$ are the diameters of the two beams at their waists. If one inserts these expressions for q_1 and q_2 into (42) and equates the imaginary parts, one obtains

$$\frac{d_1 - f}{d_2 - f} = \frac{w_1^2}{w_2^2}. \quad (60)$$

Equating the real parts results in

$$(d_1 - f)(d_2 - f) = f^2 - f_0^2 \quad (61)$$

where

$$f_0 = \pi w_1 w_2 / \lambda. \quad (62)$$

Note that the characteristic length f_0 is defined by the waist diameters of the beams to be matched. Except for the term f_0^2 , which goes to zero for infinitely small wavelengths, (61) resembles Newton's imaging formula of geometrical optics.

Any lens with a focal length $f > f_0$ can be used to perform the matching transformation. Once f is chosen, the distances d_1 and d_2 have to be adjusted to satisfy the matching formulas [10]

$$d_1 = f \pm \frac{w_1}{w_2} \sqrt{f^2 - f_0^2},$$

$$d_2 = f \pm \frac{w_2}{w_1} \sqrt{f^2 - f_0^2}. \quad (63)$$

These relations are derived by combining (60) and (61). In (63) one can choose either both plus signs or both minus signs for matching.

It is often useful to introduce the confocal parameters b_1 and b_2 into the matching formulas. They are defined by the waist diameters of the two systems to be matched

$$b_1 = 2\pi w_1^2/\lambda, \quad b_2 = 2\pi w_2^2/\lambda. \quad (64)$$

Using these parameters one gets for the characteristic length f_0

$$f_0^2 = \frac{1}{4} b_1 b_2, \quad (65)$$

and for the matching distances

$$d_1 = f \pm \frac{1}{2} b_1 \sqrt{(f^2/f_0^2) - 1},$$

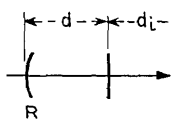
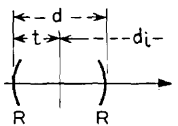
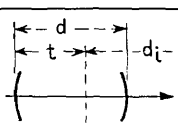
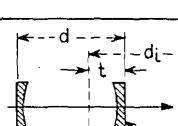
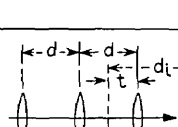
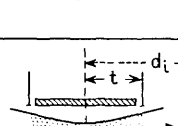
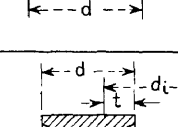
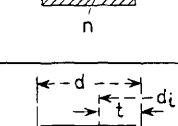
$$d_2 = f \pm \frac{1}{2} b_2 \sqrt{(f^2/f_0^2) - 1}. \quad (66)$$

Note that in this form of the matching formulas, the wavelength does not appear explicitly.

Table II lists, for quick reference, formulas for the two important parameters of beams that emerge from various

TABLE II

FORMULAS FOR THE CONFOCAL PARAMETER AND THE LOCATION OF BEAM WAIST FOR VARIOUS OPTICAL STRUCTURES

NO	OPTICAL SYSTEM	$\frac{1}{2}b = \pi w_0^2/\lambda$	t
1		$\sqrt{d(R-d)}$	—
2		$\frac{1}{2} \sqrt{d(2R-d)}$	$\frac{1}{2} d$
3		$\frac{\sqrt{d(R_1-d)(R_2-d)(R_1+R_2-d)}}{R_1+R_2-2d}$	$\frac{d(R_2-d)}{R_1+R_2-2d}$
4		$\frac{R \sqrt{d(2R-d)}}{2R+d(n^2-1)}$	$\frac{ndR}{2R+d(n^2-1)}$
5		$\frac{1}{2} \sqrt{d(4f-d)}$	$\frac{1}{2} d$
6		$\frac{1}{2} d$	$\frac{1}{2} d$
7		$\frac{d}{2n}$	$\frac{d}{2n}$
8		$\frac{nR \sqrt{d(2R-d)}}{2n^2R-d(n^2-1)}$	$\frac{dR}{2n^2R-d(n^2-1)}$

optical structures commonly encountered. They are the confocal parameter b and the distance t which gives the waist location of the emerging beam. System No. 1 is a resonator formed by a flat mirror and a spherical mirror of radius R . System No. 2 is a resonator formed by two equal spherical mirrors. System No. 3 is a resonator formed by mirrors of unequal curvature. System No. 4

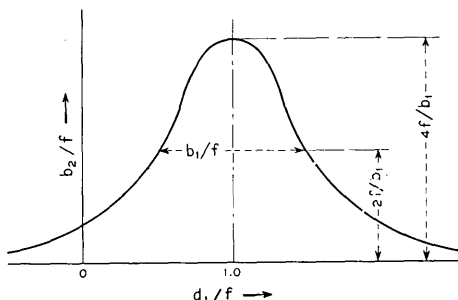


Fig. 12. The confocal parameter b_2 as a function of the lens-waist spacing d_1 .

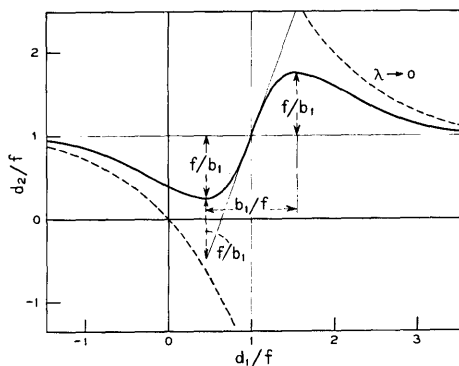


Fig. 13. The waist spacing d_2 as a function of the lens-waist spacing d_1 .

is, again, a resonator formed by two equal spherical mirrors, but with the reflecting surfaces deposited on plano-concave optical plates of index n . These plates act as negative lenses and change the characteristics of the emerging beam. This lens effect is assumed not present in Systems Nos. 2 and 3. System No. 5 is a sequence of thin lenses of equal focal lengths f . System No. 6 is a system of two irises with equal apertures spaced at a distance d . Shown are the parameters of a beam that will pass through both irises with the least possible beam diameter. This is a beam which is "confocal" over the distance d . This beam will also pass through a tube of length d with the optimum clearance. (The tube is also indicated in the figure.) A similar situation is shown in System No. 7, which corresponds to a beam that is confocal over the length d of optical material of index n . System No. 8 is a spherical mirror resonator filled with material of index n , or an optical material with curved end surfaces where the beam passing through it is assumed to have phase fronts that coincide with these surfaces.

When one designs a matching system, it is useful to know the accuracy required of the distance adjustments. The discussion below indicates how the parameters b_2 and d_2 change when b_1 and f are fixed and the lens spacing d_1 to the waist of the input beam is varied. Equations (60) and (61) can be solved for b_2 with the result [9]

$$b_2/f = \frac{b_1/f}{(1 - d_1/f)^2 + (b_1/2f)^2}. \quad (67)$$

This means that the parameter b_2 of the beam emerging from the lens changes with d_1 according to a Lorentzian functional form as shown in Fig. 12. The Lorentzian is centered at $d_1=f$ and has a width of b_1 . The maximum value of b_2 is $4f^2/b_1$.

If one inserts (67) into (60) one gets

$$1 - d_2/f = \frac{1 - d_1/f}{(1 - d_1/f)^2 + (b_1/2f)^2} \quad (68)$$

which shows the change of d_2 with d_1 . The change is reminiscent of a dispersion curve associated with a Lorentzian as shown in Fig. 13. The extrema of this curve occur at the halfpower points of the Lorentzian. The slope of the curve at $d_1=f$ is $(2f/b_1)^2$. The dashed curves in the figure correspond to the geometrical optics imaging relation between d_1 , d_2 , and f [20].

3.7 Circle Diagrams

The propagation of Gaussian laser beams can be represented graphically on a circle diagram. On such a diagram one can follow a beam as it propagates in free space or passes through lenses, thereby affording a graphic solution of the mode matching problem. The circle diagrams for beams are similar to the impedance charts, such as the Smith chart. In fact there is a close analogy between transmission-line and laser-beam problems, and there are analog electric networks for every optical system [17].

The first circle diagram for beams was proposed by Collins [18]. A dual chart was discussed in [19]. The basis for the derivation of these charts are the beam propagation laws discussed in Section 3.2. One combines (17) and (19) and eliminates q to obtain

$$\left(\frac{\lambda}{\pi w^2} + j \frac{1}{R}\right) \left(\frac{\pi w_0^2}{\lambda} - jz\right) = 1. \quad (69)$$

This relation contains the four quantities w , R , w_0 , and z which were used to describe the propagation of Gaussian beams in Section 3.2. Each pair of these quantities can be expressed in complex variables W and Z :

$$W = \frac{\lambda}{\pi w^2} + j \frac{1}{R}$$

$$Z = \frac{\pi w_0^2}{\lambda} - jz = b/2 - jz, \quad (70)$$

where b is the confocal parameter of the beam. For these variables (69) defines a conformal transformation

$$W = 1/Z. \quad (71)$$

The two dual circle diagrams are plotted in the complex planes of W and Z , respectively. The W -plane diagram [18] is shown in Fig. 14 where the variables $\lambda/\pi w^2$ and $1/R$ are plotted as axes. In this plane the lines of constant $b/2 = \pi w_0^2/\lambda$ and the lines of constant z of the Z plane appear as circles through the origin. A beam is represented by a circle of constant b , and the beam parameters w and R at a distance z from the beam waist can be easily read

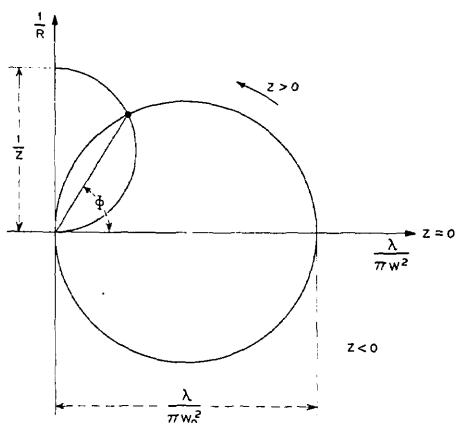


Fig. 14. Geometry for the W -plane circle diagram.

such transformation makes it possible to use the Smith chart for determining complex mismatch coefficients for Gaussian beams [20]. Other circle diagrams include those for optical resonators [21] which allow the graphic determination of certain parameters of the resonator modes.

4. LASER RESONATORS (FINITE APERTURE)

4.1 General Mathematical Formulation

In this section aperture diffraction effects due to the finite size of the mirrors are taken into account; these effects were neglected in the preceding sections. There, it was mentioned that resonators used in laser oscillators usually take the form of an open structure consisting of a pair of mirrors facing each other. Such a structure with finite mirror apertures is intrinsically lossy and, unless energy is supplied to it continuously, the electromagnetic field in it will decay. In this case a mode of the resonator is a *slowly decaying* field configuration whose relative distribution does not change with time [4]. In a laser oscillator the active medium supplies enough energy to overcome the losses so that a steady-state field can exist. However, because of nonlinear gain saturation the medium will exhibit less gain in those regions where the field is high than in those where the field is low, and so the oscillating modes of an active resonator are expected to be somewhat different from the decaying modes of the passive resonator. The problem of an active resonator filled with a saturable-gain medium has been solved recently [22], [23], and the computed results show that if the gain is not too large the resonator modes are essentially unperturbed by saturation effects. This is fortunate as the results which have been obtained for the passive resonator can also be used to describe the active modes of laser oscillators.

The problem of the open resonator is a difficult one and a rigorous solution is yet to be found. However, if certain simplifying assumptions are made, the problem becomes tractable and physically meaningful results can be obtained. The simplifying assumptions involve essentially the quasi-optic nature of the problem; specifically, they are 1) that the dimensions of the resonator are large compared to the wavelength and 2) that the field in the resonator is substantially transverse electromagnetic (TEM). So long as those assumptions are valid, the Fresnel-Kirchhoff formulation of Huygens' principle can be invoked to obtain a pair of integral equations which relate the fields of the two opposing mirrors. Furthermore, if the mirror separation is large compared to mirror dimensions and if the mirrors are only slightly curved, the two orthogonal Cartesian components of the vector field are essentially uncoupled, so that separate scalar equations can be written for each component. The solutions of these scalar equations yield resonator modes which are uniformly polarized in one direction. Other polarization configurations can be constructed from the uniformly polarized modes by linear superposition.

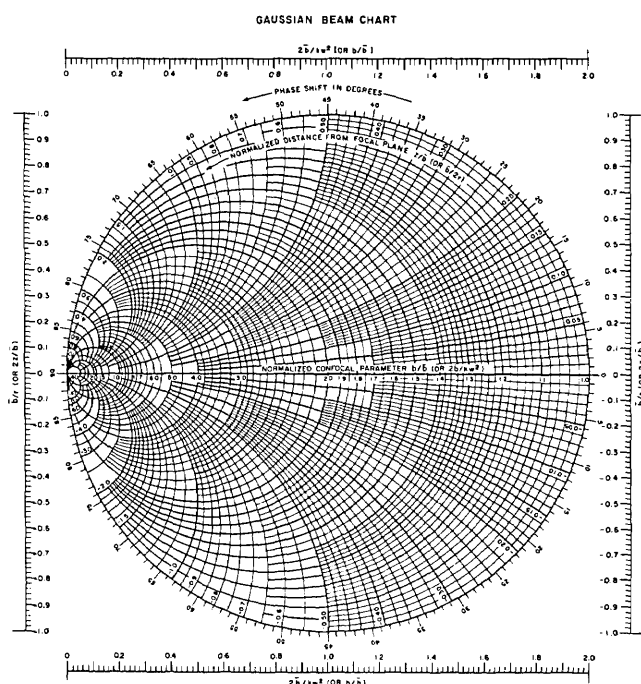


Fig. 15. The Gaussian beam chart. Both W -plane and Z -plane circle diagram are combined into one.

from the diagram. When the beam passes through a lens the phase front is changed according to (40) and a new beam is formed, which implies that the incoming and outgoing beams are connected in the diagram by a vertical line of length $1/f$. The angle Φ shown in the figure is equal to the phase shift experienced by the beam as given by (29); this is easily shown using (23).

The dual diagram [19] is plotted in the Z plane. The sets of circles in both diagrams have the same form, and only the labeling of the axes and circles is different. In Fig. 15 both diagrams are unified in one chart. The labels in parentheses correspond to the Z -plane diagram, and \bar{b} is a normalizing parameter which can be arbitrarily chosen for convenience.

One can plot various other circle diagrams which are related to the above by conformal transformations. One

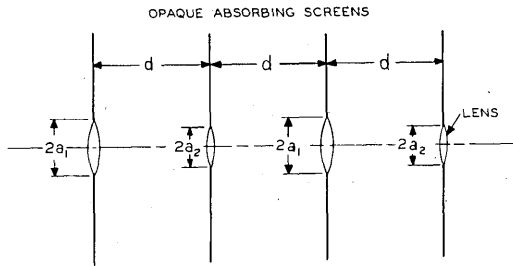
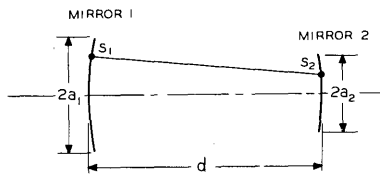


Fig. 16. Geometry of a spherical-mirror resonator with finite mirror apertures and the equivalent sequence of lenses set in opaque absorbing screens.

In deriving the integral equations, it is assumed that a traveling TEM wave is reflected back and forth between the mirrors. The resonator is thus analogous to a transmission medium consisting of apertures or lenses set in opaque absorbing screens (see Fig. 16). The fields at the two mirrors are related by the equations [24]

$$\begin{aligned}\gamma^{(1)}E^{(1)}(s_1) &= \int_{S_2} K^{(2)}(s_1, s_2)E^{(2)}(s_2)dS_2 \\ \gamma^{(2)}E^{(2)}(s_2) &= \int_{S_1} K^{(1)}(s_2, s_1)E^{(1)}(s_1)dS_1\end{aligned}\quad (72)$$

where the integrations are taken over the mirror surfaces S_2 and S_1 , respectively. In the above equations the subscripts and superscripts one and two denote mirrors one and two; s_1 and s_2 are symbolic notations for transverse coordinates on the mirror surface, e.g., $s_1=(x_1, y_1)$ and $s_2=(x_2, y_2)$ or $s_1=(r_1, \phi_1)$ and $s_2=(r_2, \phi_2)$; $E^{(1)}$ and $E^{(2)}$ are the relative field distribution functions over the mirrors; $\gamma^{(1)}$ and $\gamma^{(2)}$ give the attenuation and phase shift suffered by the wave in transit from one mirror to the other; the kernels $K^{(1)}$ and $K^{(2)}$ are functions of the distance between s_1 and s_2 and, therefore, depend on the mirror geometry; they are equal [$K^{(1)}(s_2, s_1)=K^{(2)}(s_1, s_2)$] but, in general, are not symmetric [$K^{(1)}(s_2, s_1)\neq K^{(1)}(s_1, s_2)$, $K^{(2)}(s_1, s_2)\neq K^{(2)}(s_2, s_1)$].

The integral equations given by (72) express the field at each mirror in terms of the reflected field at the other; that is, they are single-transit equations. By substituting one into the other, one obtains the double-transit or round-trip equations, which state that the field at each mirror must reproduce itself after a round trip. Since the kernel for each of the double-transit equations is symmetric [24], it follows [25] that the field distribution functions corresponding to the different mode orders are orthogonal over their respective mirror surfaces; that is

$$\begin{aligned}\int_{S_1} E_m^{(1)}(s_1)E_n^{(1)}(s_1)dS_1 &= 0, \quad m \neq n \\ \int_{S_2} E_m^{(2)}(s_2)E_n^{(2)}(s_2)dS_2 &= 0, \quad m \neq n\end{aligned}\quad (73)$$

where m and n denote different mode orders. It is to be noted that the orthogonality relation is non-Hermitian and is the one that is generally applicable to lossy systems.

4.2 Existence of Solutions

The question of the existence of solutions to the resonator integral equations has been the subject of investigation by several authors [26]–[28]. They have given rigorous proofs of the existence of eigenvalues and eigenfunctions for kernels which belong to resonator geometries commonly encountered, such as those with parallel-plane and spherically curved mirrors.

4.3 Integral Equations for Resonators with Spherical Mirrors

When the mirrors are spherical and have rectangular or circular apertures, the two-dimensional integral equations can be separated and reduced to one-dimensional equations which are amenable to solution by either analytical or numerical methods. Thus, in the case of rectangular mirrors [4]–[6], [24], [29], [30], the one-dimensional equations in Cartesian coordinates are the same as those for infinite-strip mirrors; for the x coordinate, they are

$$\begin{aligned}\gamma_x^{(1)}u^{(1)}(x_1) &= \int_{-a_2}^{a_2} K(x_1, x_2)u^{(2)}(x_2)dx_2 \\ \gamma_x^{(2)}u^{(2)}(x_2) &= \int_{-a_1}^{a_1} K(x_1, x_2)u^{(1)}(x_1)dx_1\end{aligned}\quad (74)$$

where the kernel K is given by

$$\begin{aligned}K(x_1, x_2) &= \sqrt{\frac{j}{\lambda d}} \\ &\cdot \exp \left\{ -\frac{jk}{2d}(g_1x_1^2 + g_2x_2^2 - 2x_1x_2) \right\}.\end{aligned}\quad (75)$$

Similar equations can be written for the y coordinate, so that $E(x, y)=u(x)v(y)$ and $\gamma=\gamma_x\gamma_y$. In the above equation a_1 and a_2 are the half-widths of the mirrors in the x direction, d is the mirror spacing, k is $2\pi/\lambda$, and λ is the wavelength. The radii of curvature of the mirrors R_1 and R_2 are contained in the factors

$$\begin{aligned}g_1 &= 1 - \frac{d}{R_1} \\ g_2 &= 1 - \frac{d}{R_2}.\end{aligned}\quad (76)$$

For the case of circular mirrors [4], [31], [32] the equations are reduced to the one-dimensional form by using

cylindrical coordinates and by assuming a sinusoidal azimuthal variation of the field; that is, $E(r, \phi) = R_l(r)e^{-j l \phi}$. The radial distribution functions $R_l^{(1)}$ and $R_l^{(2)}$ satisfy the one-dimensional integral equations:

$$\gamma_l^{(1)} R_l^{(1)}(r_1) \sqrt{r_1} = \int_0^{a_2} K_l(r_1, r_2) R_l^{(2)}(r_2) \sqrt{r_2} dr_2$$

$$\gamma_l^{(2)} R_l^{(2)}(r_2) \sqrt{r_2} = \int_0^{a_1} K_l(r_1, r_2) R_l^{(1)}(r_1) \sqrt{r_1} dr_1 \quad (77)$$

where the kernel K_l is given by

$$K_l(r_1, r_2) = \frac{j^{l+1}}{d} J_l \left(k \frac{r_1 r_2}{d} \right) \sqrt{r_1 r_2} \cdot \exp \left\{ -\frac{j k}{2d} (g_1 r_1^2 + g_2 r_2^2) \right\} \quad (78)$$

and J_l is a Bessel function of the first kind and l th order. In (77), a_1 and a_2 are the radii of the mirror apertures and d is the mirror spacing; the factors g_1 and g_2 are given by (76).

Except for the special case of the confocal resonator [5] ($g_1 = g_2 = 0$), no exact analytical solution has been found for either (74) or (77), but approximate methods and numerical techniques have been employed with success for their solutions. Before presenting results, it is appropriate to discuss two important properties which apply in general to resonators with spherical mirrors; these are the properties of "equivalence" and "stability."

4.4 Equivalent Resonator Systems

The equivalence properties [24], [33] of spherical-mirror resonators are obtained by simple algebraic manipulations of the integral equations. First, it is obvious that the mirrors can be interchanged without affecting the results; that is, the subscripts and superscripts one and two can be interchanged. Second, the diffraction loss and the intensity pattern of the mode remain invariant if both g_1 and g_2 are reversed in sign; the eigenfunctions E and the eigenvalues γ merely take on complex conjugate values. An example of such equivalent systems is that of parallel-plane ($g_1 = g_2 = 1$) and concentric ($g_1 = g_2 = -1$) resonator systems.

The third equivalence property involves the Fresnel number N and the stability factors G_1 and G_2 , where

$$N = \frac{a_1 a_2}{\lambda d}$$

$$G_1 = g_1 \frac{a_1}{a_2}$$

$$G_2 = g_2 \frac{a_2}{a_1} \quad (79)$$

If these three parameters are the same for any two resonators, then they would have the same diffraction loss, the

same resonant frequency, and mode patterns that are scaled versions of each other. Thus, the equivalence relations reduce greatly the number of calculations which are necessary for obtaining the solutions for the various resonator geometries.

4.5 Stability Condition and Diagram

Stability of optical resonators has been discussed in Section 2 in terms of geometrical optics. The stability condition is given by (8). In terms of the stability factors G_1 and G_2 , it is

$$0 < G_1 G_2 < 1$$

or

$$0 < g_1 g_2 < 1. \quad (80)$$

Resonators are stable if this condition is satisfied and unstable otherwise.

A stability diagram [6], [24] for the various resonator geometries is shown in Fig. 4 where g_1 and g_2 are the coordinate axes and each point on the diagram represents a particular resonator geometry. The boundaries between stable and unstable (shaded) regions are determined by (80), which is based on geometrical optics. The fields of the modes in stable resonators are more concentrated near the resonator axes than those in unstable resonators and, therefore, the diffraction losses of unstable resonators are much higher than those of stable resonators. The transition, which occurs near the boundaries, is gradual for resonators with small Fresnel numbers and more abrupt for those with large Fresnel numbers. The origin of the diagram represents the confocal system with mirrors of equal curvature ($R_1 = R_2 = d$) and is a point of lowest diffraction loss for a given Fresnel number. The fact that a system with minor deviations from the ideal confocal system may become unstable should be borne in mind when designing laser resonators.

4.6 Modes of the Resonator

The transverse field distributions of the resonator modes are given by the eigenfunctions of the integral equations. As yet, no exact analytical solution has been found for the general case of arbitrary G_1 and G_2 , but *approximate* analytical expressions have been obtained to describe the fields in *stable* spherical-mirror resonators [5], [6]. These approximate eigenfunctions are the same as those of the optical beam modes which are discussed in Section 2; that is, the field distributions are given *approximately* by Hermite-Gaussian functions for rectangular mirrors [5], [6], [34], and by Laguerre-Gaussian functions for circular mirrors [6], [7]. The designation of the resonator modes is given in Section 3.5. (The modes are designated as TEM_{mnq} for rectangular mirrors and TEM_{plq} for circular mirrors.) Figure 7 shows photographs of some of the rectangular mode patterns of a

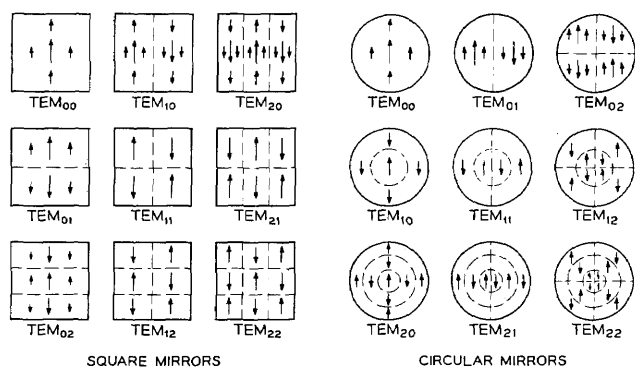


Fig. 17. Linearly polarized resonator mode configurations for square and circular mirrors.

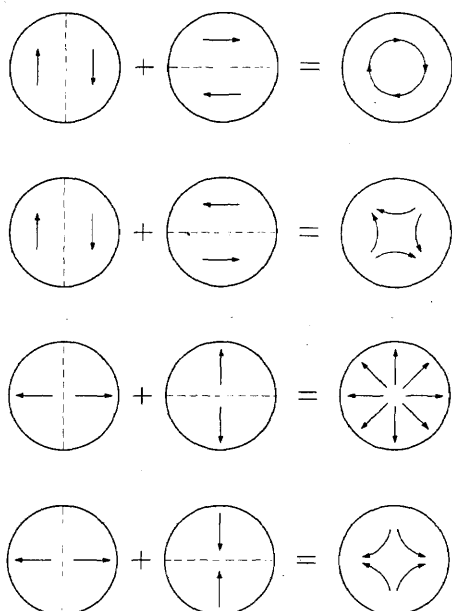


Fig. 18. Synthesis of different polarization configurations from the linearly polarized TEM_{01} mode.

laser. Linearly polarized mode configurations for square mirrors and for circular mirrors are shown in Fig. 17. By combining two orthogonally polarized modes of the same order, it is possible to synthesize other polarization configurations; this is shown in Fig. 18 for the TEM_{01} mode.

Field distributions of the resonator modes for any value of G could be obtained numerically by solving the integral equations either by the method of successive approximations [4], [24], [31] or by the method of kernel expansion [30], [32]. The former method of solution is equivalent to calculating the transient behavior of the resonator when it is excited initially with a wave of arbitrary distribution. This wave is assumed to travel back and forth between the mirrors of the resonator, undergoing changes from transit to transit and losing energy by diffraction. After many transits a quasi steady-state condition is attained where the fields for successive transits

differ only by a constant multiplicative factor. This steady-state *relative* field distribution is then an eigenfunction of the integral equations and is, in fact, the field distribution of the mode that has the lowest diffraction loss for the symmetry assumed (e.g., for even or odd symmetry in the case of infinite-strip mirrors, or for a given azimuthal mode index number l in the case of circular mirrors); the constant multiplicative factor is the eigenvalue associated with the eigenfunction and gives the diffraction loss and the phase shift of the mode. Although this simple form of the iterative method gives only the lower order solutions, it can, nevertheless, be modified to yield higher order ones [24], [35]. The method of kernel expansion, however, is capable of yielding both low-order and high-order solutions.

Figures 19 and 20 show the relative field distributions of the TEM_{00} and TEM_{01} modes for a resonator with a pair of identical, circular mirrors ($N=1$, $a_1=a_2$, $g_1=g_2=g$) as obtained by the numerical iterative method. Several curves are shown for different values of g , ranging from zero (confocal) through one (parallel-plane) to 1.2 (convex, unstable). By virtue of the equivalence property discussed in Section 4.4, the curves are also applicable to resonators with their g values reversed in sign, provided the sign of the ordinate for the phase distribution is also reversed. It is seen that the field is most concentrated near the resonator axis for $g=0$ and tends to spread out as $|g|$ increases. Therefore, the diffraction loss is expected to be the least for confocal resonators.

Figure 21 shows the relative field distributions of some of the low order modes of a Fabry-Perot resonator with (parallel-plane) circular mirrors ($N=10$, $a_1=a_2$, $g_1=g_2=1$) as obtained by a modified numerical iterative method [35]. It is interesting to note that these curves are not very smooth but have small wiggles on them, the number of which are related to the Fresnel number. These wiggles are entirely absent for the confocal resonator and appear when the resonator geometry is unstable or nearly unstable. Approximate expressions for the field distributions of the Fabry-Perot resonator modes have also been obtained by various analytical techniques [36], [37]. They are represented to first order, by sine and cosine functions for infinite-strip mirrors and by Bessel functions for circular mirrors.

For the special case of the confocal resonator ($g_1=g_2=0$), the eigenfunctions are self-reciprocal under the *finite* Fourier (infinite-strip mirrors) or Hankel (circular mirrors) transformation and exact analytical solutions exist [5], [38]–[40]. The eigenfunctions for infinite-strip mirrors are given by the prolate spheroidal wave functions and, for circular mirrors, by the generalized prolate spheroidal or hyperspheroidal wave functions. For large Fresnel numbers these functions can be closely approximated by Hermite-Gaussian and Laguerre-Gaussian functions which are the eigenfunctions for the beam modes.

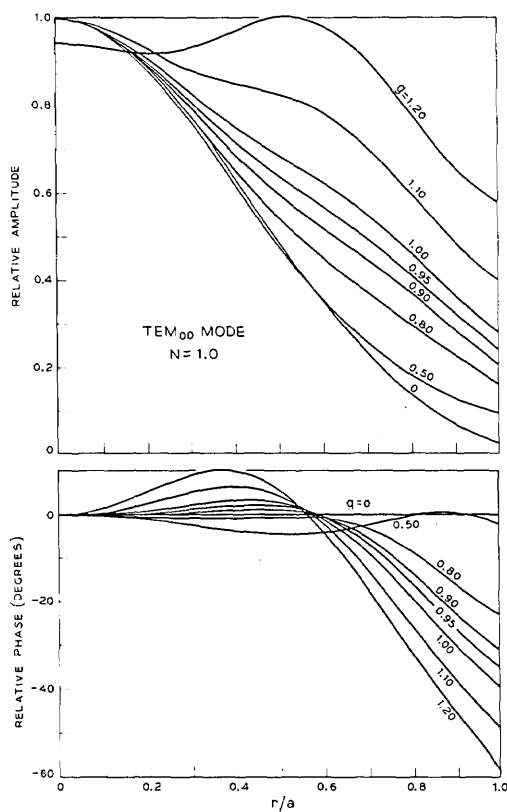


Fig. 19. Relative field distributions of the TEM_{00} mode for a resonator with circular mirrors ($N=1$).

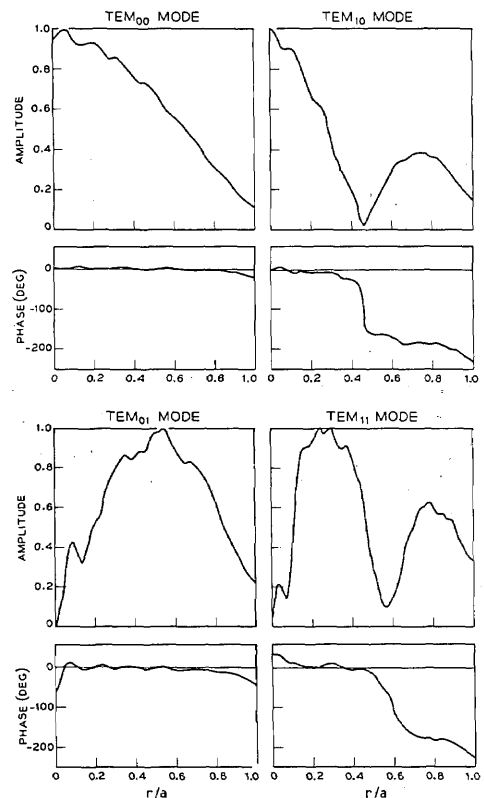


Fig. 21. Relative field distributions of four of the low order modes of a Fabry-Perot resonator with (parallel-plane) circular mirrors ($N=10$).

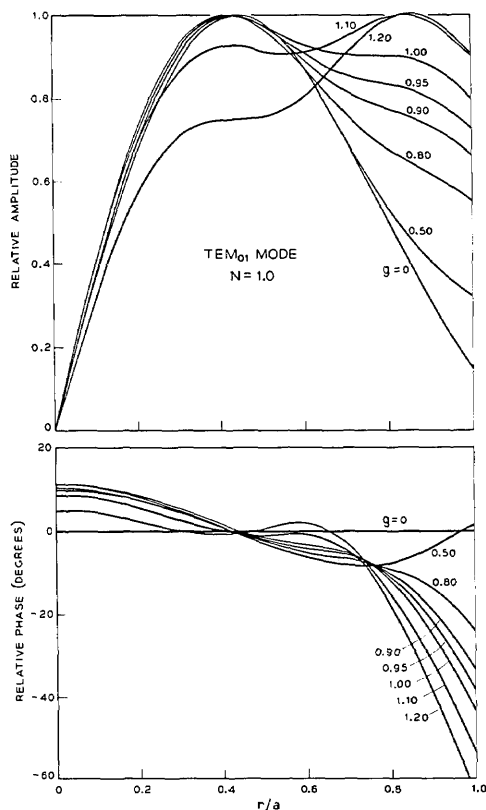


Fig. 20. Relative field distributions of the TEM_{01} mode for a resonator with circular mirrors ($N=1$).

4.7 Diffraction Losses and Phase Shifts

The diffraction loss α and the phase shift β for a particular mode are important quantities in that they determine the Q and the resonant frequency of the resonator for that mode. The diffraction loss is given by

$$\alpha = 1 - |\gamma|^2 \quad (81)$$

which is the fractional energy lost per transit due to diffraction effects at the mirrors. The phase shift is given by

$$\beta = \text{angle of } \gamma \quad (82)$$

which is the phase shift suffered (or enjoyed) by the wave in transit from one mirror to the other, in addition to the geometrical phase shift which is given by $2\pi d/\lambda$. The eigenvalue γ in (81) and (82) is the appropriate γ for the mode under consideration. If the total resonator loss is small, the Q of the resonator can be approximated by

$$Q = \frac{2\pi d}{\lambda \alpha_t} \quad (83)$$

where α_t , the total resonator loss, includes losses due to diffraction, output coupling, absorption, scattering, and other effects. The resonant frequency ν is given by

$$\nu/\nu_0 = (q + 1) + \beta/\pi \quad (84)$$

where q , the longitudinal mode order, and ν_0 , the fundamental beat frequency, are defined in Section 3.5.

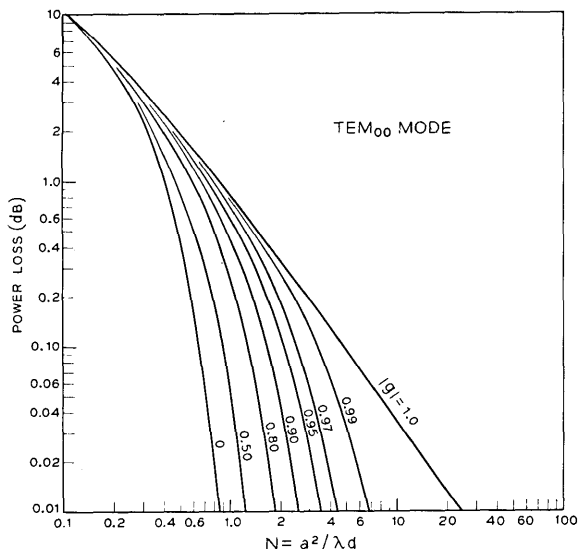


Fig. 22. Diffraction loss per transit (in decibels) for the TEM_{00} mode of a stable resonator with circular mirrors.

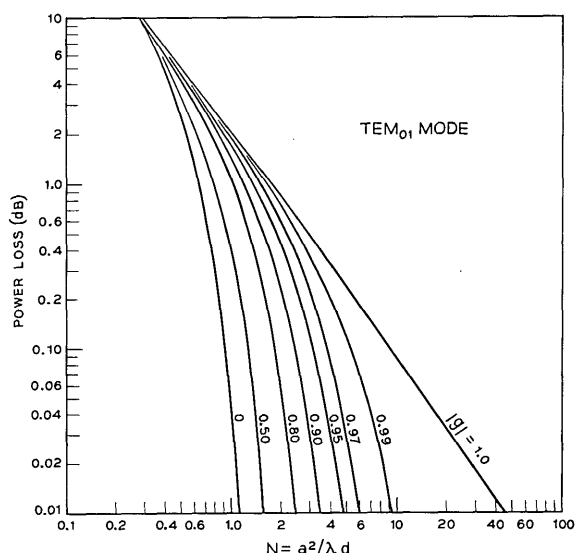


Fig. 23. Diffraction loss per transit (in decibels) for the TEM_{01} mode of a stable resonator with circular mirrors.

The diffraction losses for the two lowest order (TEM_{00} and TEM_{01}) modes of a stable resonator with a pair of identical, circular mirrors ($a_1 = a_2$, $g_1 = g_2 = g$) are given in Figs. 22 and 23 as functions of the Fresnel number N and for various values of g . The curves are obtained by solving (77) numerically using the method of successive approximations [31]. Corresponding curves for the phase shifts are shown in Figs. 24 and 25. The horizontal portions of the phase shift curves can be calculated from the formula

$$\begin{aligned} \beta &= (2p + l + 1) \arccos \sqrt{g_1 g_2} \\ &= (2p + l + 1) \arccos g, \quad \text{for } g_1 = g_2 \end{aligned} \quad (85)$$

which is equal to the phase shift for the beam modes derived in Section 3.5. It is to be noted that the loss curves are applicable to both positive and negative values of g

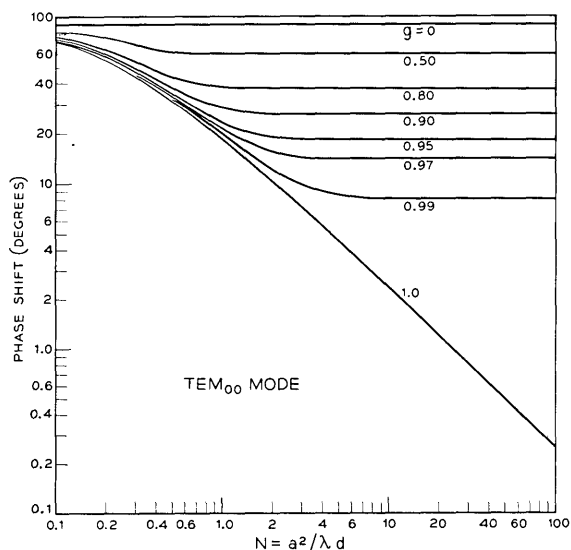


Fig. 24. Phase shift per transit for the TEM_{00} mode of a stable resonator with circular mirrors.

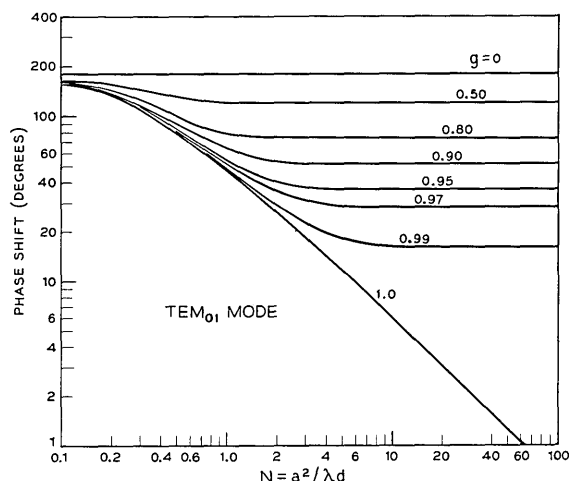


Fig. 25. Phase shift per transit for the TEM_{01} mode of a stable resonator with circular mirrors.

while the phase-shift curves are for positive g only; the phase shift for negative g is equal to 180 degrees minus that for positive g .

Analytical expressions for the diffraction loss and the phase shift have been obtained for the special cases of parallel-plane ($g = 1.0$) and confocal ($g = 0$) geometries when the Fresnel number is either very large (small diffraction loss) or very small (large diffraction loss) [36], [38], [39], [41], [42]. In the case of the parallel-plane resonator with circular mirrors, the approximate expressions valid for large N , as derived by Vainshtein [36], are

$$\alpha = 8\kappa_{pl} \frac{\delta(M + \delta)}{[(M + \delta)^2 + \delta^2]^2} \quad (86)$$

$$\beta = \left(\frac{M}{4\delta}\right) \alpha \quad (87)$$

where $\delta = 0.824$, $M = \sqrt{8\pi N}$, and κ_{pl} is the $(p+1)$ th zero of the Bessel function of order l . For the confocal resonator with circular mirrors, the corresponding expressions are [39]

$$\alpha = \frac{2\pi(8\pi N)^{2p+l+1}e^{-4\pi N}}{p!(p+l+1)!} \left[1 + O\left(\frac{1}{2\pi N}\right) \right] \quad (88)$$

$$\beta = (2p+l+1) \frac{\pi}{2} \quad (89)$$

Similar expressions exist for resonators with infinite-strip or rectangular mirrors [36], [39]. The agreement between the values obtained from the above formulas and those from numerical methods is excellent.

The loss of the lowest order (TEM₀₀) mode of an *unstable* resonator is, to first order, independent of the mirror size or shape. The formula for the loss, which is based on geometrical optics, is [12]

$$\alpha = 1 \pm \frac{1 - \sqrt{1 - (g_1 g_2)^{-1}}}{1 + \sqrt{1 - (g_1 g_2)^{-1}}} \quad (90)$$

where the plus sign in front of the fraction applies for g values lying in the first and third quadrants of the stability diagram, and the minus sign applies in the other two quadrants. Loss curves (plotted vs. N) obtained by solving the integral equations numerically have a ripply behavior which is attributable to diffraction effects [24], [43]. However, the average values agree well with those obtained from (90).

5. CONCLUDING REMARKS

Space limitations made it necessary to concentrate the discussion of this article on the basic aspects of laser beams and resonators. It was not possible to include such interesting topics as perturbations of resonators, resonators with tilted mirrors, or to consider in detail the effect of nonlinear, saturating host media. Also omitted was a discussion of various resonator structures other than those formed of spherical mirrors, e.g., resonators with corner cube reflectors, resonators with output holes, or fiber resonators. Another important, but omitted, field is that of mode selection where much research work is currently in progress. A brief survey of some of these topics is given in [44].

REFERENCES

- [1] R. H. Dicke, "Molecular amplification and generation systems and methods," U. S. Patent 2 851 652, September 9, 1958.
- [2] A. M. Prokhorov, "Molecular amplifier and generator for sub-millimeter waves," *JETP (USSR)*, vol. 34, pp. 1658-1659, June 1958; *Sov. Phys. JETP*, vol. 7, pp. 1140-1141, December 1958.
- [3] A. L. Schawlow and C. H. Townes, "Infrared and optical masers," *Phys. Rev.*, vol. 29, pp. 1940-1949, December 1958.
- [4] A. G. Fox and T. Li, "Resonant modes in an optical maser," *Proc. IRE (Correspondence)*, vol. 48, pp. 1904-1905, November 1960; "Resonant modes in a maser interferometer," *Bell Sys. Tech. J.*, vol. 40, pp. 453-488, March 1961.
- [5] G. D. Boyd and J. P. Gordon, "Confocal multimode resonator for millimeter through optical wavelength masers," *Bell Sys. Tech. J.*, vol. 40, pp. 489-508, March 1961.
- [6] G. D. Boyd and H. Kogelnik, "Generalized confocal resonator theory," *Bell Sys. Tech. J.*, vol. 41, pp. 1347-1369, July 1962.
- [7] G. Goubau and F. Schermer, "On the guided propagation of electromagnetic wave beams," *IRE Trans. on Antennas and Propagation*, vol. AP-9, pp. 248-256, May 1961.
- [8] J. R. Pierce, "Modes in sequences of lenses," *Proc. Nat'l Acad. Sci.*, vol. 47, pp. 1808-1813, November 1961.
- [9] G. Goubau, "Optical relations for coherent wave beams," in *Electromagnetic Theory and Antennas*. New York: Macmillan, 1963, pp. 907-918.
- [10] H. Kogelnik, "Imaging of optical mode—Resonators with internal lenses," *Bell Sys. Tech. J.*, vol. 44, pp. 455-494, March 1965.
- [11] —, "On the propagation of Gaussian beams of light through lenslike media including those with a loss or gain variation," *Appl. Opt.*, vol. 4, pp. 1562-1569, December 1965.
- [12] A. E. Siegman, "Unstable optical resonators for laser applications," *Proc. IEEE*, vol. 53, pp. 277-287, March 1965.
- [13] W. Brower, *Matrix Methods in Optical Instrument Design*. New York: Benjamin, 1964. E. L. O'Neill, *Introduction to Statistical Optics*. Reading, Mass.: Addison-Wesley, 1963.
- [14] M. Bertolotti, "Matrix representation of geometrical properties of laser cavities," *Nuovo Cimento*, vol. 32, pp. 1242-1257, June 1964. V. P. Bykov and L. A. Vainshtein, "Geometrical optics of open resonators," *JETP (USSR)*, vol. 47, pp. 508-517, August 1964. B. Macke, "Laser cavities in geometrical optics approximation," *J. Phys. (Paris)*, vol. 26, pp. 104A-112A, March 1965. W. K. Kahn, "Geometric optical derivation of formula for the variation of the spot size in a spherical mirror resonator," *Appl. Opt.*, vol. 4, pp. 758-759, June 1965.
- [15] J. R. Pierce, *Theory and Design of Electron Beams*. New York: Van Nostrand, 1954, p. 194.
- [16] H. Kogelnik and W. W. Rigrod, "Visual display of isolated optical-resonator modes," *Proc. IRE (Correspondence)*, vol. 50, p. 220, February 1962.
- [17] G. A. Deschamps and P. E. Mast, "Beam tracing and applications," in *Proc. Symposium on Quasi-Optics*. New York: Polytechnic Press, 1964, pp. 379-395.
- [18] S. A. Collins, "Analysis of optical resonators involving focusing elements," *Appl. Opt.*, vol. 3, pp. 1263-1275, November 1964.
- [19] T. Li, "Dual forms of the Gaussian beam chart," *Appl. Opt.*, vol. 3, pp. 1315-1317, November 1964.
- [20] T. S. Chu, "Geometrical representation of Gaussian beam propagation," *Bell Sys. Tech. J.*, vol. 45, pp. 287-299, February 1966.
- [21] J. P. Gordon, "A circle diagram for optical resonators," *Bell Sys. Tech. J.*, vol. 43, pp. 1826-1827, July 1964. M. J. Offerhaus, "Geometry of the radiation field for a laser interferometer," *Philips Res. Rept.*, vol. 19, pp. 520-523, December 1964.
- [22] H. Statz and C. L. Tang, "Problem of mode deformation in optical masers," *J. Appl. Phys.*, vol. 36, pp. 1816-1819, June 1965.
- [23] A. G. Fox and T. Li, "Effect of gain saturation on the oscillating modes of optical masers," *IEEE J. of Quantum Electronics*, vol. QE-2, p. lxii, April 1966.
- [24] —, "Modes in a maser interferometer with curved and tilted mirrors," *Proc. IEEE*, vol. 51, pp. 80-89, January 1963.
- [25] F. B. Hildebrand, *Methods of Applied Mathematics*. Englewood Cliffs, N. J.: Prentice Hall, 1952, pp. 412-413.
- [26] D. J. Newman and S. P. Morgan, "Existence of eigenvalues of a class of integral equations arising in laser theory," *Bell Sys. Tech. J.*, vol. 43, pp. 113-126, January 1964.
- [27] J. A. Cochran, "The existence of eigenvalues for the integral equations of laser theory," *Bell Sys. Tech. J.*, vol. 44, pp. 77-88, January 1965.
- [28] H. Hochstadt, "On the eigenvalue of a class of integral equations arising in laser theory," *SIAM Rev.*, vol. 8, pp. 62-65, January 1966.
- [29] D. Gloge, "Calculations of Fabry-Perot laser resonators by scattering matrices," *Arch. Elect. Ubertrag.*, vol. 18, pp. 197-203, March 1964.
- [30] W. Streifer, "Optical resonator modes—rectangular reflectors of spherical curvature," *J. Opt. Soc. Am.*, vol. 55, pp. 868-877, July 1965.
- [31] T. Li, "Diffraction loss and selection of modes in maser resonators with circular mirrors," *Bell Sys. Tech. J.*, vol. 44, pp. 917-932, May-June, 1965.
- [32] J. C. Heurtley and W. Streifer, "Optical resonator modes—

- circular reflectors of spherical curvature," *J. Opt. Soc. Am.*, vol. 55, pp. 1472-1479, November 1965.
- [33] J. P. Gordon and H. Kogelnik, "Equivalence relations among spherical mirror optical resonators," *Bell Sys. Tech. J.*, vol. 43, pp. 2873-2886, November 1964.
- [34] F. Schwering, "Reiterative wave beams of rectangular symmetry," *Arch. Elect. Übertrag.*, vol. 15, pp. 555-564, December 1961.
- [35] A. G. Fox and T. Li, to be published.
- [36] L. A. Vainshtein, "Open resonators for lasers," *JETP (USSR)*, vol. 44, pp. 1050-1067, March 1963; *Sov. Phys. JETP*, vol. 17, pp. 709-719, September 1963.
- [37] S. R. Barone, "Resonances of the Fabry-Perot laser," *J. Appl. Phys.*, vol. 34, pp. 831-843, April 1963.
- [38] D. Slepian and H. O. Pollak, "Prolate spheroidal wave functions, Fourier analysis and uncertainty—I," *Bell Sys. Tech. J.*, vol. 40, pp. 43-64, January 1961.
- [39] D. Slepian, "Prolate spheroidal wave functions, Fourier anal-

- ysis and uncertainty—IV: Extensions to many dimensions; generalized prolate spheroidal functions," *Bell Sys. Tech. J.*, vol. 43, pp. 3009-3057, November 1964.
- [40] J. C. Heurtley, "Hyperspheroidal functions—optical resonators with circular mirrors," in *Proc. Symposium on Quasi-Optics*. New York: Polytechnic Press, 1964, pp. 367-375.
- [41] S. R. Barone and M. C. Newstein, "Fabry-Perot resonances at small Fresnel numbers," *Appl. Opt.*, vol. 3, p. 1194, October 1964.
- [42] L. Bergstein and H. Schachter, "Resonant modes of optic cavities of small Fresnel numbers," *J. Opt. Soc. Am.*, vol. 55, pp. 1226-1233, October 1965.
- [43] A. G. Fox and T. Li, "Modes in a maser interferometer with curved mirrors," in *Proc. Third International Congress on Quantum Electronics*. New York: Columbia University Press, 1964, pp. 1263-1270.
- [44] H. Kogelnik, "Modes in optical resonators," in *Lasers*, A. K. Levine, Ed. New York: Dekker, 1966.

Modes, Phase Shifts, and Losses of Flat-Roof Open Resonators

P. F. CHECCACCI, ANNA CONSORTINI, AND ANNAMARIA SCHEGGI

Abstract—The integral equation of a "flat-roof resonator" is solved by the Fox and Li method of iteration in a number of particular cases.

Mode patterns, phase shifts, and power losses are derived. A good overall agreement is found with the approximate theory previously developed by Toraldo di Francia.

Some experimental tests carried out on a microwave model give a further confirmation of the theoretical predictions.

I. INTRODUCTION

A PARTICULAR type of open resonator terminated by roof reflectors with very small angles, the so-called "flat-roof resonator" (Fig. 1) was recently described by Toraldo di Francia [1].

The mathematical approach consisted in considering the solutions of the wave equation (for the electric or magnetic field) in the two halves of a complete "diamond cavity" whose normal cross section is shown in Fig. 2, ignoring the fact that the reflectors are finite.

The two half-cavities were referred to cylindrical coordinates centered at G and H , respectively, and solutions were given in terms of high-order cylindrical waves. The field in the two half-cavities was matched over the median

Manuscript received May 4, 1966. The research reported here was supported in part by the Air Force Cambridge Research Laboratories through the European Office of Aerospace Research (OAR), U. S. Air Force, under Contract AF 61(052)-871.

The authors are with the Centro Microonde, Consiglio Nazionale delle Ricerche, Florence, Italy.

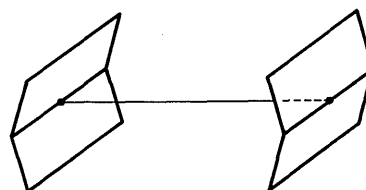


Fig. 1. The flat-roof resonator.

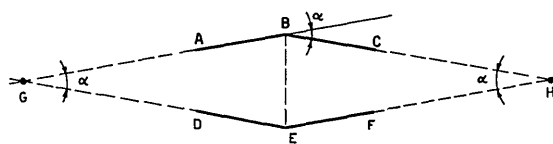


Fig. 2. The diamond cavity.

plane BE by simply requiring that this plane coincide with a node or an antinode. Obviously the α angle of the roof must be so small that the curvature of the nodal or antinodal surfaces can be neglected. Due to the high order of the cylindrical waves, the field in the central region of the cavity approaches the form of a standing wave between the two roof reflectors, while it decays so rapidly from the central region toward the vertices G and H , that the absence of the complete metal walls of the diamond outside the resonator will have very little importance. This treatment, although approximate, allowed the author to understand how the resonator actually worked